Boost Inverter for Switched Reluctance Motor Drive without Additional Inductor

Satoshi Ohtaki
Dept. of Electrical, Electronics, and Information Engineering
Nagaoka University of Technology
Nagaoka, Japan
s213112@stn.nagaokaut.ac.jp

Hirotaka Kato
Dept. of Electrical, Electronics, and Information Engineering
Nagaoka University of Technology
Nagaoka, Japan
s203139@stn.nagaokaut.ac.jp

Hiroki Watanabe
Dept. of Electrical, Electronics, and Information Engineering
Nagaoka University of Technology
Nagaoka, Japan
hwatanabe@vos.nagaokaut.ac.jp

Jun-ichi Itoh
Dept. of Electrical, Electronics, and Information Engineering
Nagaoka University of Technology
Nagaoka, Japan
itoh@vos.nagaokaut.ac.jp

***Abstract*— This paper proposes a novel topology of a boost inverter for a switched reluctance motor (SRM) without an additional inductor. In addition, this paper realizes a design method for a boost-up capacitor. The SRM drive is required to suppress a radial force ripple caused by acoustic noise and vibration. The seamless current control entails a rapid current control response. However, the current control response is limited by the DC link voltage. Moreover, the di/dt is increased due to a back electromagnetic voltage of the SRM at high speed. Applying the additional inductor achieves an increase of the maximum voltage but also provides an increase of the volume. The proposed inverter only adds a boost-up capacitor to the DC part without an additional inductor to boost a DC link voltage. The boost-up capacitor is designed to minimize the volume. The proposed circuit achieves a boost operation at all operating points. The phase current follows the current command, thanks to the boost function under various operating conditions. The capacitor voltage ripple matches the design value with an error rate of -13.5%. The validity of the proposed design method of the boost-up capacitor is confirmed.**

Keywords—boost inverter, switched reluctance motor, radial force ripple, acoustic noise.

I. INTRODUCTION

Recently, a system miniaturization has been required to reduce the manufacturing cost of electric vehicles (EVs). An integrated motor drive (IMD) system has attracted attention for its high power density, lightweight, and improved electromagnetic compatibility (EMC)[1-3]. The IMD is a single-unit structure that integrates the motor and inverter into a system. The IMD system eliminates the connection cables between the motor and the inverter. The Permanent magnet synchronous motor (PMSM) is widely adopted in IMD[3]. The PMSM has distinguished its high power density and high efficiency for the drive system. On the other hand, the PMSM has high manufacturing costs and high thermal sensitivity due to a rare-earth-element. Thus, a switched reluctance motor (SRM) is expected for the IMD system. The SRM has the advantage of rare-earth-element-flee, robustness, and low manufacturing cost due to the consisting of an iron core and windings[4-5]. Furthermore, The SRM is suited to high-speed drives by the super torque/inertia ratio due to the salient pole structure.

The SRM rotates continuously by magnetizing or demagnetizing of the winding current at the appropriate timing. An asymmetrical half-bridge (AHB) converter is generally used to drive the SRM during the positive torque section. On the other hand, the SRM drives cause significant acoustic noise and vibration due to the radial force ripple, which occurs by switching the excitation phase. Thus, a control method with a seamless current command applies to the SRM in order to suppress the radial force ripple[6]. However, the seamless current command requires a more rapid current control response compared with the pulse current command. In addition, the di/dt is increased depending on the back electromagnetic voltage (EMF) of the SRM at high speed. A high voltage is required to follow the current command. Hence, the AHB converter is added to a boost function with an additional inductor to the DC part in order to boost a phase voltage because the di/dt is limited to the DC link voltage. Although the additional inductor results in an increase of the system size.

Many topologies have been studied to boost the DC link voltage using only a boost-up capacitor[7-10]. These topologies boost a capacitor voltage using the regenerative energy of the armature inductance of the SRM. The di/dt is increased by applying the capacitor voltage. These topologies with a boost-up capacitor are classified into the capacitor connected to the DC part in series[7-8] and parallel[9-10]. The series type only utilizes the pulse current command and applies the voltage, which is the capacitor voltage added to the DC link voltage into the SRM. On the other hand, the seamless current command is not utilized due to the capacitor voltage control considering the pulse current command only. The parallel type[9] is available for various current commands and does not use additional switching devices for the boost function. However, this topology cannot operate regeneration area. The other parallel type[10] only utilizes the pulse current command, although this topology allows the regenerative operation.

This paper proposes a novel topology of a boost inverter for the SRM, which consists of the AHB converter and boost function using the capacitor. The proposed inverter achieves regenerative operation and drive with the seamless current command. Additional switches control the voltage of the boost-up capacitor. In addition, this paper presents the design method for the boost-up capacitor in the proposed inverter.

First, the topology of the proposed inverter including the operation principle and the capacitor voltage control is described. Next, the proposed design method of the boost-up capacitor is explained. In the experimental results, the boost operation of the proposed inverter is realized in all operation areas. The effectiveness of the proposed method is confirmed.

II. Proposed Boost Inverter

A. Operation Principle

Figure 1 shows the configuration of the proposed inverter. The proposed inverter has the same circuit for each phase. Each phase of the proposed inverter consists of an AHB converter and two switches. The proposed inverter assumes the hysteresis current control to the SRM by switching S_{dc} and S_c. In addition, the switches are controlled to keep the V_c constant independently. The details of the control method are explained in subsections II-B.

Figure 2 shows the operation modes of the proposed inverter. The proposed inverter switches an applying voltage depending on the operation area where the required voltage is larger than E_{dc}. The proposed inverter applies $\pm E_{dc}$ to the motor inductor L_x with a switching pattern Mode 1 and Mode 2, respectively. Similarly, the proposed inverter applies $\pm V_c$ using Mode 3 and Mode 4, respectively.

B. Voltage Control of Boost-up Capacitor

Figure 3 shows the voltage command using a seamless current control at high speed. The waveform of the voltage command at one electric period is generated from the motor parameter. The area in which the voltage command exceeds E_{dc} is defined as a "boost area" in this paper. The capacitor voltage increases when the voltage command is negative in the boost area. Similarly, the capacitor voltage decreases in the case of the positive voltage command in the boost area.

The proposed boost function includes the voltage control of the boost-up capacitor to keep V_c constant in one electrical period. This paper focuses on the electric charge of the boost-up capacitor Q_c. The V_c fluctuates due to the charging and discharging of the capacitor with Mode 3 and Mode 4. The Q_c is expressed as in (1),

$$Q_c(\theta_e) = \frac{V_c}{C_{\mathrm{bst}}} = \frac{1}{\omega_e}\int_0^{2\pi} i_c(\theta_e)\mathrm{d}\theta_e \quad \begin{cases} i_c(\theta_e) = i_x(\theta_e), & \text{Mode3} \\ i_c(\theta_e) = -i_x(\theta_e), & \text{Mode4} \\ i_c(\theta_e) = 0, & \text{Other} \end{cases} \qquad (1),$$

where $i_x(\theta_e)$ is the phase current, C_{bst} is the boost-up capacitance, ω_e and θ_e are the electric position and the electric rotation speed, i_c is the capacitor current. The condition is expressed as in (2) to keep V_c constant at one electrical period.

$$Q_c(0, 2\pi) = 0 \qquad (2),$$

Fig. 4 shows the electric charge of the boost-up capacitor in the proposed inverter. Q_c increases in the boost area when the voltage command of Fig.3 applies to the SRM with the proposed inverter. In order to be satisfied with (2), The voltage control under the hysteresis current control necessaries applying $\pm V_c$ in the outside boost area as shown in Fig.4. The voltage control applies $\pm E_{dc}$ to the SRM in the area where the difference of Q_c became zero.

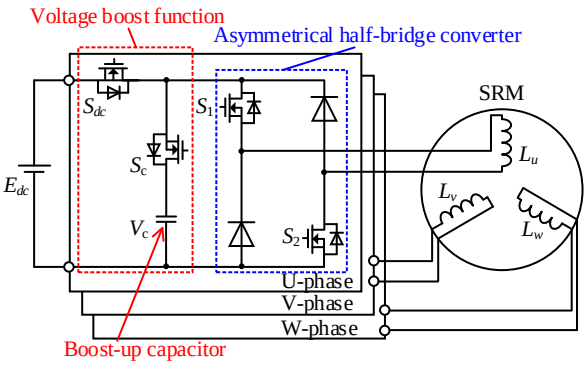

Fig.1 Configuration of proposed inverter.

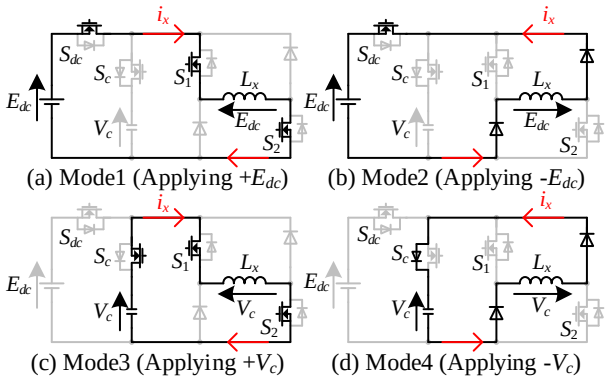

(a) Mode1 (Applying $+E_{dc}$) (b) Mode2 (Applying $-E_{dc}$)

(c) Mode3 (Applying $+V_c$) (d) Mode4 (Applying $-V_c$)

Fig.2 Operation modes of proposed inverter.

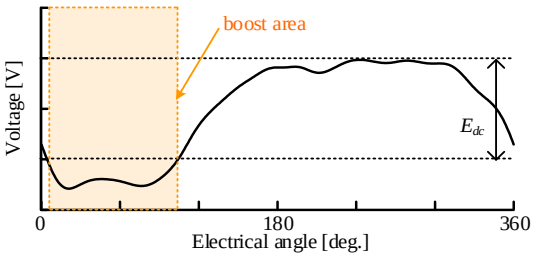

Fig.3 Waveforms of voltage command applying seamless current control.

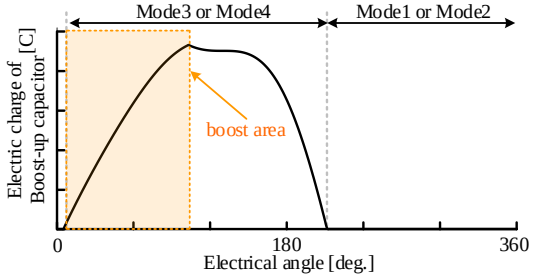

Fig.4 Electric charge of boost-up capacitor with proposed inverter

Figure 5 indicates the determination flowchart of S_{dc} and S_c. to control the capacitor voltage. The flowchart is executed every control period to determine the switching pattern. Vc and Cbst calculate equation (2) in the implementation. The details of the C_{bst} derivation are explained in section III. Mode 3 and Mode 4 are selected not only the boost area but also the period that is derived to satisfy (2). Note that S_{dc} and S_c operate complementary.

III. Design of Boost-up Capacitor

Figure 6 illustrates the design flowchart of the boost-up capacitor. The capacitor is designed to minimize capacitance and boost operation simultaneously in all operation areas.

First, the voltage command using the seamless current control is derived at a desired operating point (N, T). The voltage command is calculated by a mathematical model of the SRM based on the Finite Element Method (FEM) analysis result[6]. The radial force $F_r(i, \theta_e)$, the torque $F_\tau(i, \theta_e)$, and the voltage command $V^*(i, \theta_e)$ are approximated as follows by Fourier series and polynomial function.

$$\begin{cases} F_T(i,\theta_e) = \sum_{j=0}^{J}\left\{\left(\sum_{m=0}^{M} K_{Tm}\cdot i^m\right)\cdot\sin(j\theta_e)\right\} \\ F_R(i,\theta_e) = \sum_{j=0}^{J}\left\{\left(\sum_{m=0}^{M} K_{Rm}\cdot i^m\right)\cdot\cos(j\theta_e)\right\} \\ V^*(i,\theta_e) = \omega_e\cdot\sum_{j=0}^{J}\left\{\left(\sum_{m=0}^{M} K_{Vm}\cdot i^m\right)\cdot\sin(j\theta_e)\right\} \end{cases} \quad (3),$$

where K_{Tm}, K_{Rm}, and K_{Vm} are coefficients of a polynomial function, and the $i(\theta_e)$ is phase current. Note that the order of each approximation J and M are set to be 10. The $i(\theta_e)$ is defined as in (4).

$$i(\theta_e) = \sum_{l=0}^{L} i_l \sin(l\cdot\theta_e) \quad (4),$$

where i_l is the harmonic amplitude of the phase current, and the order L is 3. The phase current of (4) is optimized to satisfy the constant condition below. (i) The radial force ripple is less than the desired ripple. (ii) The torque command matches the torque average of (3). (iii) The root-mean-square of phase current is minimization.

Next, the fluctuation of the electric charge of the boost-up capacitor Q_c is calculated based on the derived $V^*(i, \theta_e)$. The peak-to-peak value of the Q_c in one electrical period Q_{c_diff} is shown as (5).

$$Q_{c\_diff} = \max\left[Q_c(0,2\pi)\right] - \min\left[Q_c(0,2\pi)\right] \quad (5),$$

In order to design the capacitance in which the Q_c is the most significant fluctuation in all operating points, the Q_{c_diff} updates when the Q_{c_diff} is higher than the maximum of the $Q_{c\_diff\_max}$ at the last operating points. Note that the operating points are ignored in case of not satisfying (2). The voltage command of the boost-up capacitor V_c^* is obtained, such as the flow calculation of $Q_{c\_diff\_max}$. The highest voltage in the derived $V^*(i, \theta_e)$ is calculated from (6).

$$V_c^* = \max\left[\left|V^*\right|\right] \quad (6),$$

In order to design the voltage command of the maximum value in all operating points, the V_c^* updates when the V^*_c is higher than the maximum value of the $V^*_{c\_max}$ at the last operating points. The calculation $Q_{c\_diff\_max}$ and $V^*_{c\_max}$ continues until the highest $Q_{c\_diff\_max}$ and $V^*_{c\_max}$ are determined in all operating points.

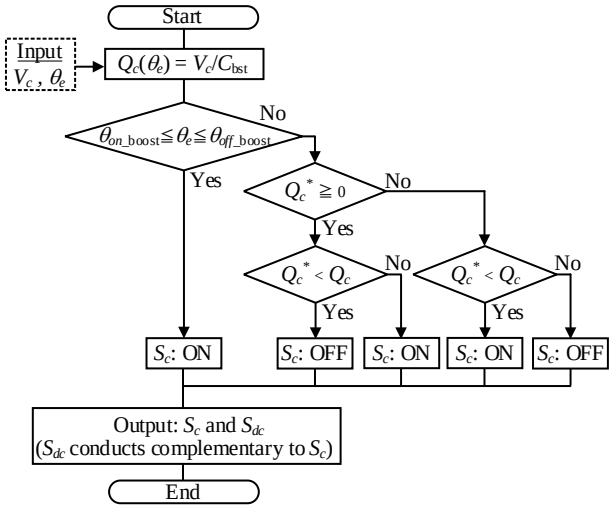

Fig.5 Determination flowchart of switching pattern for capacitor voltage control.

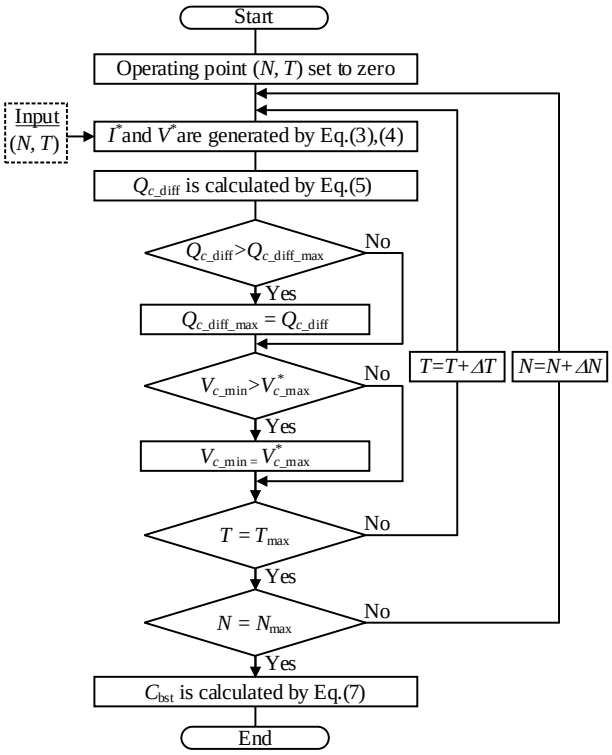

Fig.6 Design flow chart of boost-up capacitor.

Finally, the boost-up capacitance C_{bst} is determined. The capacitance is generally small in case of a large voltage ripple of the capacitor. However, there are trade-off relationship between the capacitor voltage ripple and the withstand voltage of the switching device V_{device}. Thus, a boost-up capacitor has to be designed to minimize capacitance under the limitation of V_{device}. The design equation of C_{bst} is expressed as in (7).

$$C_{bst} = \frac{Q_{c\_diff\_max}}{V_{device} - V^*_{c\_max}} \quad (7),$$

In this paper, the $V_{c\_max}^*$ and the V_{device} are set to 270 V and 310 V against the E_{dc}=150 V, respectively. The 50 μF of the capacitor is selected by (7) since the $Q_{c\_diff\_max}$ is 193 μC.

IV. Experimental Results

In this section, the experimental system validates the steady-state response and transient response of the motor applying the proposed circuit. The effectiveness, which is the design method of the boost-up capacitor and the voltage control are demonstrated by two experimental results.

Table I shows the motor parameters of SRM. The test motor is a three-phase 18S/12P type SRM, of 1.1 kW, 2400 rpm (=1.0p.u.), and 4.38 Nm (=1.0p.u.).

Figure 7 displays the experimental system. The load motor outputs the arbitrary constant speed. Note that the bandwidth is set to 0.5 A in the hysteresis current control.

Figure 8 shows the command waveform generated by the flowchart of Fig.6. These waveforms are the current command and the voltage command at base speed and rated torque. The phase shifts half-electric period in case of regenerating. Note that the boost area is set to widely in order to easy to experiment simplicity because the S_c always turns on between two of the boost areas.

A. Steady State Response of Proposed Inverter

Figure 9 shows the comparison results of the operating waveforms when base speed and rated torque. Speed. The phase current does not follow the current command because the di/dt is limited to the DC link voltage, in Fig.9(a). The phase voltage is only applied to 150 V, even though it is the boost area. On the other hand, the phase current follows the current command accurately by the proposed circuit in the boost area, as shown in Fig.9(b). The capacitor voltage ripple in the boost area is within the designed value of 270 and 310 V. The error of 4 V occurs between the lower limit of the voltage ripple and the capacitor voltage command.

Figure 10 shows the capacitor voltage waveform at four electric periods. Fig.10 indicates the period in which the capacitor voltage keeps 270 V or not. As shown in Fig.6, the Sc always turns off when the detected capacitor voltage is less than 270 V outside the boost area. Thus, the capacitor voltage keeps 266 V because the influence of the detection error causes the error. Similarly, the capacitor voltage ripples at each period are different due to changing the section in which the capacitor voltage is charged, by detection error. Therefore, the effectiveness of the capacitor voltage control is demonstrated.

Figure 11 shows the comparison results of the operating waveforms during regenerating at base speed and rated torque. The capacitor voltage became the maximum at this operating point. Therefore, the capacitor voltage ripple is verified by the operation point, $V_{c\_diff\_max}$, used for the design method. Fig 11(a) indicates that the phase current matches the current command thanks to the boost function such as in Fig. 9(a). As shown in Fig.11(b), The capacitor voltage ripple, which is 34.6 V, matches the designed value with an error of -13.5%. Therefore, the above experiment results validate the proposed design method of the boost-up capacitor and the capacitor voltage control.

B. Transient Response of Proposed Inverter

Figure 12 shows the operating waveform of the torque step response. The torque command is changed from 0.67p.u. to 1.0p.u. at base speed. As shown in Fig.12, the phase current follows the current command accurately. The capacitor voltage waveform shows the capacitor voltage control is accurate at the transient response because the fluctuation of the capacitor voltage is within the design value in case of the torque command change.

Table I. Moter parameter of SRM.

Rated power	1.1 kW
Base speed(1.0p.u.), Max. speed	2400, 3600 rpm
Max. torque(1.0p.u.)	4.38 Nm
DC link voltage	150 V
Poles	Stator:18, Rotor:12
Resistance	0.66 Ω
Rated current(1.0p.u.)	11.5 A

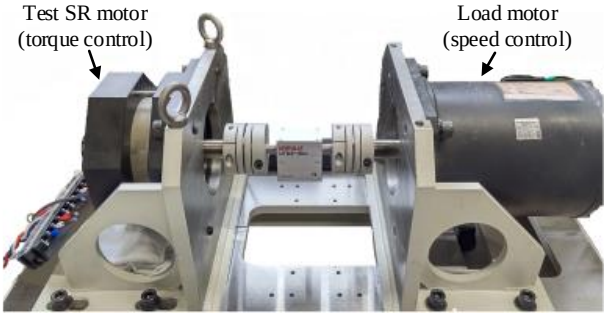

Fig. 7 Experimental system.

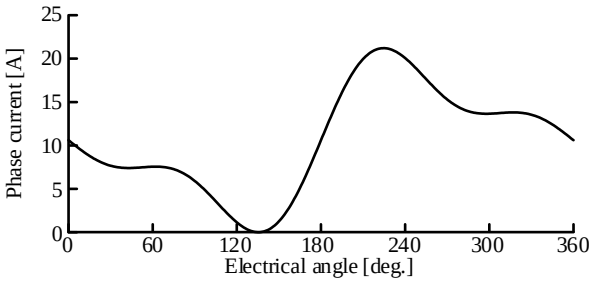

(a) Current command at motoring.

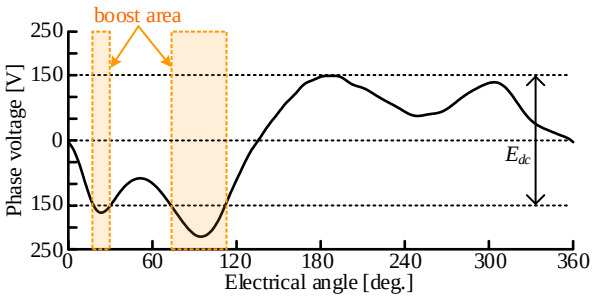

(b) Voltage command at motoring.

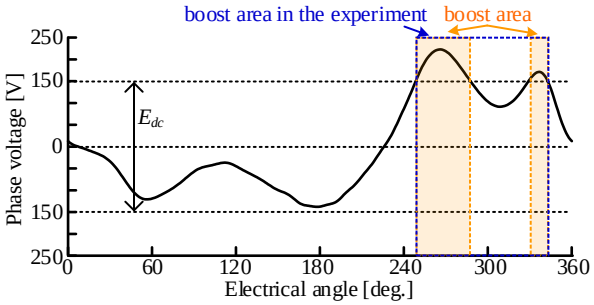

(c) Voltage command at regenerating.

Fig. 8 Command waveforms in the experiments.

V. CONCLUSION

This paper proposes the novel topology of the proposed inverter for the SRM without additional inductor. The proposed inverter consists of the AHB converter and the boost function using the capacitor. The boost-up capacitance is derived from the designed capacitor voltage ripple and the electric charge determined by the current command. The experimental results reveal the effectiveness of the capacitor voltage control in the proposed inverter since the phase current follows the command current under various conditions due to the boost function. In addition, the boost operation with the proposed inverter is realized in all operating areas. The capacitor voltage ripple matches the designed value with an error of -13.5%. Therefore, the validity of the design method of the boost-up capacitor is confirmed. In future work, the

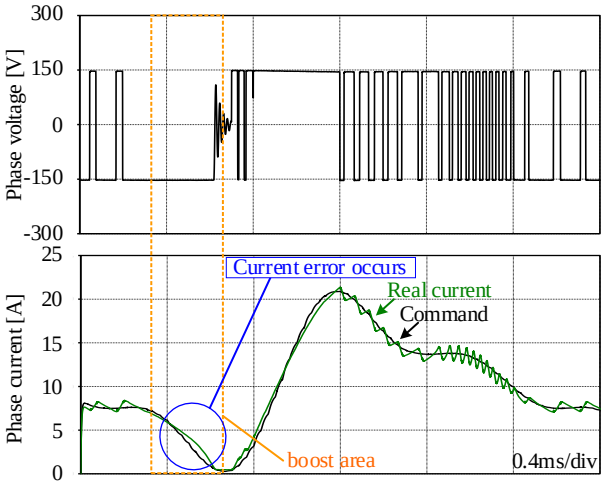

(a)Waveforms without boost function

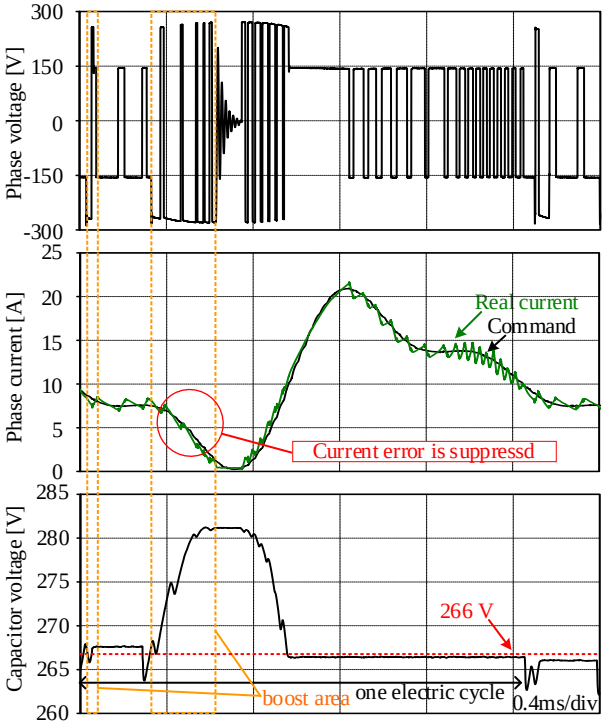

(b) Waveforms with boost function

Fig.9 Operating waveform during motoring. at 1.0 torque and 1.0 speed.

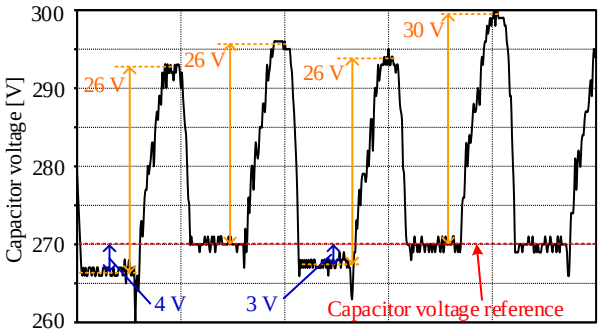

Fig.10 capacitor voltage waveforms at four electric periods.

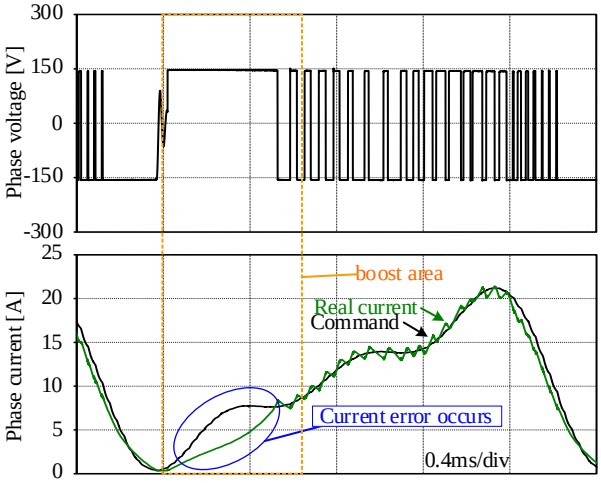

(a) Waveforms without boost function

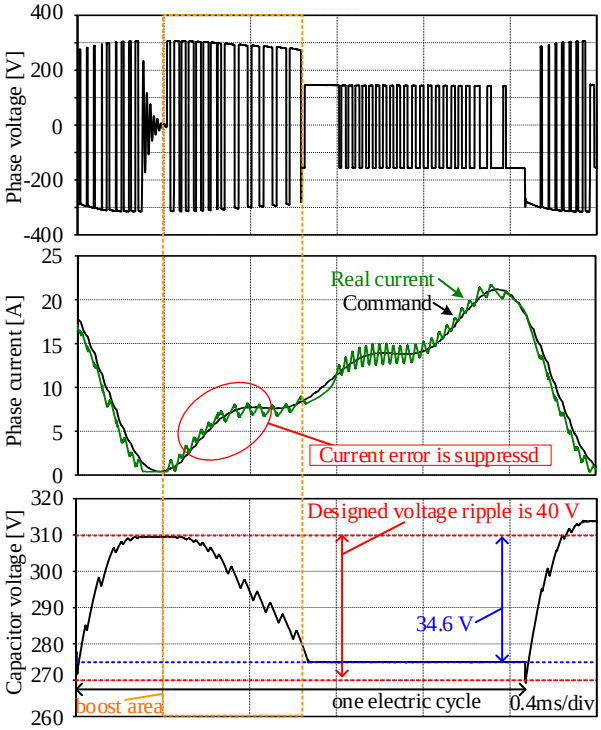

(b) Waveforms with boost function

Fig.11 Operating waveform during regenerating at 1.0 torque and 1.0 speed.

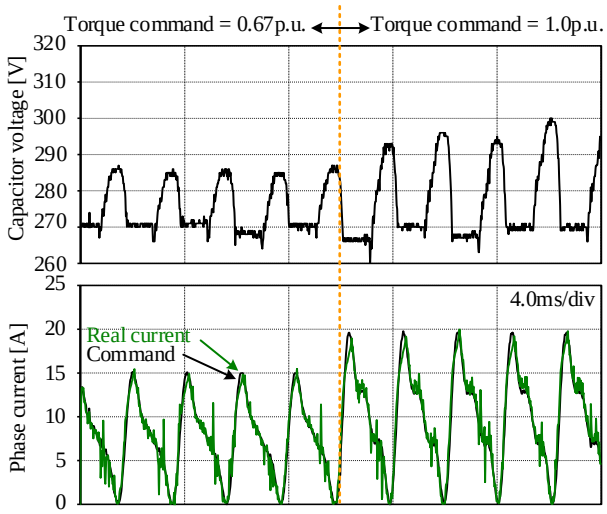

Fig.12 Operating waveform during changing torque command from 0.67p.u. to 1.0p.u.

number of devices in the boost function will be reduced, and the boost-up capacitance will be minimalized.

REFERENCES

[1] A. H. Mohamed, H. Vansompel, and P. Sergeant, "Electrothermal Design of a Discrete GaN-Based Converter for Integrated Modular Motor Drives," IEEEJ of Emerging and Selected Topics in Power Electronics, Vol.9, No.5, pp.5390-5406, 2021.

[2] A. H. Mohamed, H. Vansompel and P. Sergeant, "Polygon-Retrofitted Integrated Modular Motor Drive for Switched Reluctance Machines," IEEE Trans. on Industrial Electronics, Vol.69, No.12, pp.12469-12479, 2022.

[3] W. Lee, S. Li, D. Han, B. Sarlioglu, T. A. Minav, and M. Pieteola, "A Review of Integrated Motor Drive and Wide-Bandgap Power Electronics for High-Performance Electro-Hydrostatic Actuators," IEEE Trans. on Transportation Electrification, Vol.4, No.3, pp.684-693, 2018.

[4] T. Kumagai, H. Sakurai, T. Shioi, H. Kato, J. Itoh, K. Kusaka, T. Yamaguchi, Masayuki Nakagawa, and D.Sato, "Experimental Evaluation of Switched Reluctance Motor Made by Blanking Amorphous Alloy Foil," IEEJ Journal of Industry Applications, Vol.11, No.1, pp.117-127, 2022.

[5] S. Hirayama, and S. Takagi, "Evaluation of DC Excitation of External-Rotor-Segment-Type SRM for Power Generation," IEEJ Journal of Industry Applications, Vol.12, No.2, pp.155-161, 2023.

[6] J. Furqani, M. Kawa, K. Kiyota, and A. Chiba, "Current Waveform for Noise Reduction of a Switched Reluctance Motor under Magnetically Saturated Condition," IEEE Trans. Industrial Application, Vol.54, No.1, pp.213-222, 2018

[7] Y. Kido, N. Hoshi, A. Chiba, S. Ogasawara, and M. Takemoto, "Novel Switched Reluctance Motor Drive Circuit with Voltage Boost Function without Additional Reactor," Proceedings of the 2011 14th European Conference on Power Electronics and Applications (EPE2011), pp.1-10.

[8] R. Sugai, T. Kurishima, H. Goto, H. Funato, J. Haruna: "Optimal Design Proposal for Capacitance in Operating Area Expandable SR Motor Drive Circuit." IEEJ Journal of Industry Applications, Vol.12, No.4, pp.711-718, 2023.

[9] H. Ishikawa, H. Naitoh: "Torque Ripple Minimization for Switched Reluctance Motors Driven by a Boost Type Drive Circuit," IEEJ Journal of Industry Applications, Vol.137, No.10, pp.791-798, 2017.

[10] K. Yamaguchi, and J. Magome, "SIC-MOSFET Converter for Switched Reluctance Motors," IEEJ Trans. on Electronics, and Information and Systems, Vol.135, No.7, pp.761-768, 2014